

Synthesizing Nitrogen-Doped Core–Sheath Carbon Nanotube Films for Flexible Lithium Ion Batteries

Zhiyong Pan, Jing Ren, Guozhen Guan, Xin Fang, Binjie Wang, Seok-Gwang Doo, In Hyuk Son, Xianliang Huang, and Huisheng Peng*

Advantages in structure and property have boosted the exploration of carbon nanotubes (CNTs) for various energy storage devices.^[1–3] CNTs are widely appreciated as electrode materials due to high mechanical and electrical properties. However, these merits are rarely expressed in the form of a film where CNTs are usually randomly dispersed and interpenetrated with each other with high contact resistances.^[4–6] Therefore, aligned CNT films are prepared to eliminate the disorder and improve the charge transport along the aligned direction.^[7–9] Moreover, guest materials like platinum nanoparticles, silver nanowires and graphene sheets are introduced as functional components to better the conductivity.^[10–13] In most cases, these materials are anchored on the CNTs and are prone to aggregate, which to some extent, will interfere with the alignment. Another approach for increasing the conductivity is doping with heteroatoms—nitrogen, sulfur and boron.^[14–18] The doped atoms will facilitate the charge transport and enhance the energy storage capability of CNTs.^[19–23] Regrettably, the combination of alignment and heteroatomic doping has never been realized because it is difficult to make the heteroatom-doped CNTs into an aligned film.

Given the increasing popularity of wearable electronics, flexible energy storage devices such as lithium ion battery (LIB) have attracted intense interests. Though great efforts have been devoted to developing suitable flexible electrodes,^[24–26] the inferior electrochemical performances still impede its progress toward a large-scale production. Generally, flexible LIBs rely on traditional compounds like LiCo_2O_4 , LiMnO_2 , and $\text{LiTi}_5\text{O}_{12}$ as active materials. Therefore, their specific capacities are theoretically limited at 100–300 mAh g^{-1} .^[26–29] Silicon as an anode

material has an ultra-high specific capacity but it suffers from a severe degradation during charge and discharge processes.^[8–30] Flexible LIBs mainly from carbon-based flexible electrodes have been widely explored such as nanoporous CNTs,^[31] graphene papers,^[32] electrospun porous carbon nanofibers,^[33] and hollow CNT/carbon nanofiber composite material.^[34] However, the high contact resistance within the randomly dispersed CNTs or graphene sheets limits the full expression of their advantages. As a result, superior flexible electrodes are still under pressing demands to enhance the overall performance of flexible LIBs.

In this Communication, a new family of aligned N-doped core–sheath carbon nanotube (N-CNT) films has been synthesized and developed as flexible and effective anodes of LIBs. The N-CNT film is synthesized from a template of aligned CNT sheet by chemical vapor deposition (Figure 1a). Typically, N-doped graphene layers are coaxially grown around bare CNTs in the sheet, and the N-doped sheath can be well controlled by varying the growth time. These N-CNT films exhibit high tensile strength of 690 MPa and electrical conductivity of 410 S cm^{-1} . In particular, the N-doped graphene layer favors the intercalation of lithium ions, so they can be used as new electrodes for high-performance LIBs. They display a high capacity of 390 mAh g^{-1} that retains 97% after 200 cycles at a high rate of 4C.

To prepare the N-CNT film, aligned CNT sheets that had been drawn out of the spinnable CNT array were stacked along the CNT length on a heat-resisted ceramic framework. It was then transferred to a tube furnace to regrow the nitrogen-doped graphene layers on the outer surfaces of CNTs using acetonitrile as both nitrogen and carbon sources. At high temperature of 1060 °C, acetonitrile decomposed into C- and N-containing fragments, which were attached onto the surface of the template CNT and reformed as new graphene sheets along with the radial direction. Due to the defects introduced by the N-doping, the new grown layers were less uniform compared with original CNT walls (Figure S1, Supporting Information). The thickness of nitrogen-doped graphene was controlled by varying the reaction time (Figure 1b). The N-CNT films were compared for the reaction time of 10, 30, 60, and 90 min by scanning electron microscopy (SEM) and transmission electron microscopy (TEM) (Figure 2a–f; Figure S2–S4 (Supporting Information)). The template CNTs shared a multiwalled structure with a diameter of 17 nm. The diameters of N-CNTs were increased with increasing reaction time. For instance, they reached 25 and 220 nm in 10 and 90 min, respectively (Figure 2e). For the aligned CNT sheet, some neighboring CNTs were bundled together when they had been bridged or crossed with each other, and the nitrogen-doped graphene layer could be grown on the bundled CNTs (Figure 2g; Figure S5 and S6 (Supporting Information)).

Z. Pan, J. Ren, Dr. G. Guan, X. Fang, Dr. B. Wang,
Prof. H. Peng

State Key Laboratory of Molecular
Engineering of Polymers
Department of Macromolecular Science
and Laboratory of Advanced Materials
Fudan University
Shanghai 200438, P. R. China
E-mail: penghs@fudan.edu.cn

Dr. S.-G. Doo, Dr. I. H. Son
Energy Materials Lab
Materials Research Center
Samsung Advanced Institute of Technology
Samsung Electronics Co., LTD.
130 Samsung-ro, Suwon-si, Gyeonggi-do 443803, South Korea

Dr. X. Huang
Samsung R&D Institute China
Beijing 100028, P. R. China



DOI: 10.1002/aenm.201600271

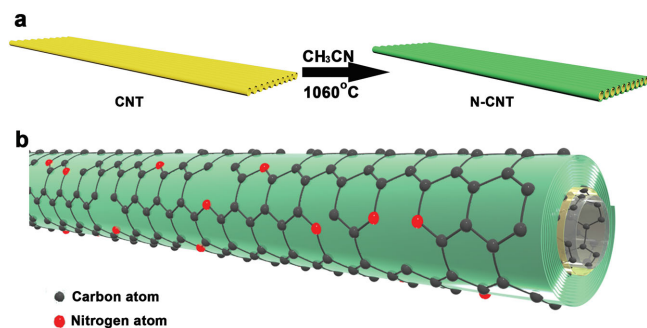


Figure 1. Schematic illustration to the synthesis of the aligned (a) N-CNT film and (b) structure of an N-CNT.

The chemical state of the N in the N-doped layer is studied by Raman spectra and X-ray photoelectron spectroscopy (XPS). Raman spectra reveal the increasing defect of the N-doped layer as the peak density of D band rose (Figure 2h; Figure S7 (Supporting Information)). The 2D band of template CNTs at 2660 cm^{-1} became almost invisible in the resulting N-CNT because the CNTs were completely covered by the N-doped graphene sheets with a lot of defects. XPS indicated that there existed three types of doping nitrogen atoms. The peaks at 398.2, 401.3, and 404.1 eV correspond to pyridinic (N1), pyrrolic (N2), and graphitic (N3) N atoms, respectively (Figure 2i). The weight percentage of nitrogen was 6% in the N-CNT film with a reaction time of 60 min (Figure S8 and S9, Supporting Information).

The free-standing CNT sheet was flexible but easily broke under deformations such as bending and twisting (Figure S10a,

Supporting Information). When the reaction time to form the nitrogen-doped graphene layer was below 30 min, it could not maintain the original morphology and tended to collapse for some parts. With the increase in reaction time to 30 and 60 min, the N-CNT films became stable and well retained the structure under bending (Figure 3a,b), and they were lightweight with densities of 0.254 and 0.796 mg cm^{-2} , respectively. The N-CNT films were also flexible (Figure 3b; Figure S10b (Supporting Information)) and strong with a tensile strength of 690 MPa (Figure 3c). Their electrical resistances along the aligned direction were only slightly increased after bending for 500 cycles (Figure S11, Supporting Information). With the further increase in the reaction time to 90 min, the N-CNT films maintained the structure but were too thick with a much decreased flexibility (Figure S10c, Supporting Information). UV-vis transmittance spectra were used to verify that the aligned structure from the templated CNT sheet was maintained in the N-CNT films (Figure S12, Supporting Information).

The aligned structure in both CNT sheet and N-CNT film gave rise to an anisotropic behavior in electrical property. The electrical resistances of both CNT sheet and N-CNT film were measured and compared in all directions (Figure 3d). For the same N-CNT film, the resistances were 25, 393, 711, 1951, and $2645\ \Omega$ in the directions of 0° , 30° , 45° , 60° , and 90° in relative to the aligned direction, respectively. As expected, due to the conjugation between lone pair electrons in nitrogen and π systems of the carbon lattice, the N-CNT film exhibited higher electrical conductivities than the CNT sheet in all directions. For instance, along the aligned direction, the electrical

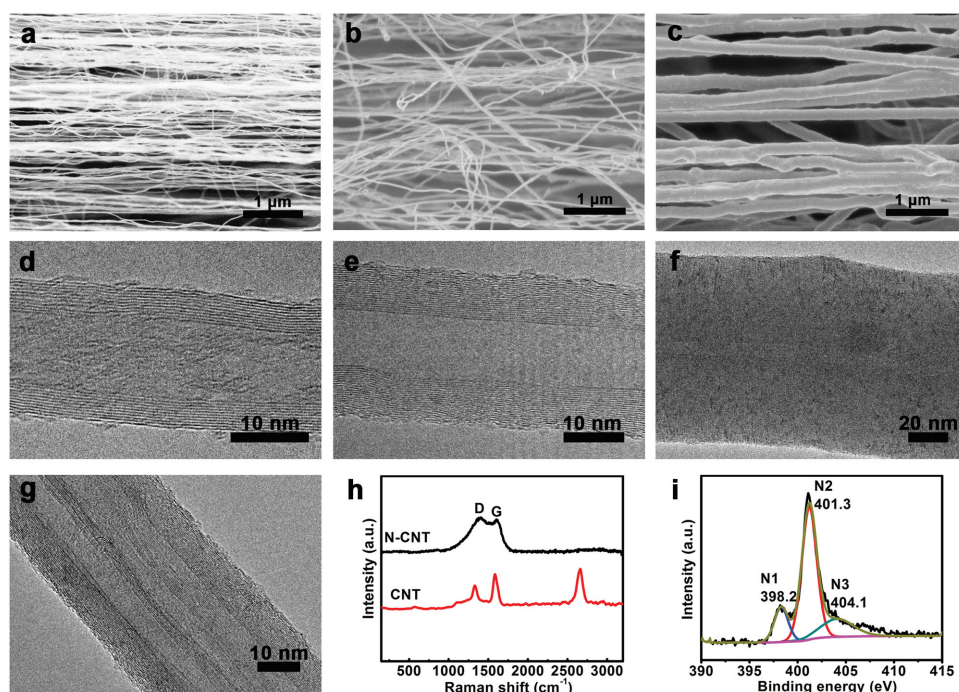


Figure 2. Structure characterization on the aligned CNT sheet before and after growth of the N-doped graphene layer. a) SEM image of CNTs. b,c) SEM images of N-CNTs with growth times of 10 and 60 min, respectively. d) TEM image of an original CNT. e,f) TEM images of N-CNTs with growth times of 10 and 60 min, respectively. g) TEM image of a multicore structure of the N-CNT. h) Raman spectra of CNT sheet and N-CNT film with growth time of 60 min. i) N 1s XPS spectra of the N-CNT film with growth time of 60 min.

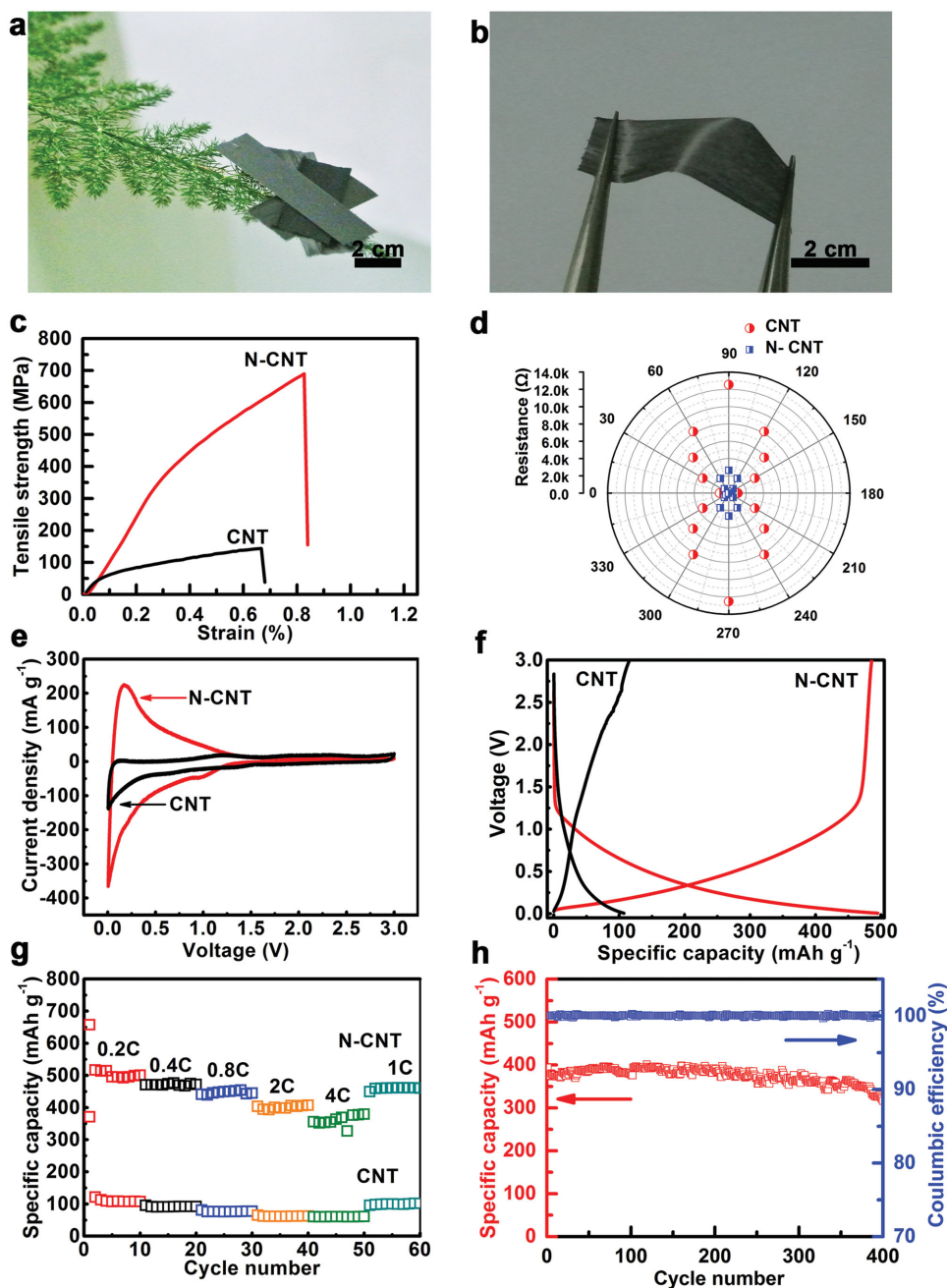


Figure 3. Property characterizations. a) Photograph of several N-CNT films on a tip of asparagus fern. b) A free-standing N-CNT film. c) Stress–strain curves of CNT sheet and N-CNT film. d) Comparison on the electrical resistance of CNT sheet and N-CNT film at different directions. The lengths were the same of 1 cm. e) Cyclic voltammograms of CNT and N-CNT at scan rate of 0.5 mV s⁻¹. f) Galvanostatic charge and discharge curves of CNTs and N-CNTs at 0.1 A g⁻¹. g) Specific capacity over cycling for CNTs and N-CNTs at different rates. h) Capacity retention and Coulombic efficiency of N-CNTs after 400 charge–discharge cycles at 4C. The N-CNT film was grown for 30 min at (b) and 60 min at (c–h), and it included 5 layers.

conductivity of the N-CNT film reached 410 S cm⁻¹, compared with 200 S cm⁻¹ in the bare CNT sheet.

To examine the electrochemical performances, the N-CNT films were used as electrodes to assemble coin cells with the use of lithium foil. Galvanostatic charge–discharge measurements had been conducted for the samples with different reaction times (Figure S13, Supporting Information). The specific discharge capacities were first increased with the increasing

reaction time to 60 min; they were then decreased with the further increase in the reaction time as the diffusion of lithium ions was suppressed by the thicker graphene layers. The highest specific capacity reached 383 mAh g⁻¹ at 60 min. Note that the template CNT sheets with five layers exhibited the peak specific capacity due to the same reason (Figure S14, Supporting Information), i.e., the specific capacities were decreased when the N-CNT films became too thick beyond five layers.

Therefore, the reaction time of 60 min and template CNT sheet of five layers are studied below unless specified otherwise.

Cyclic voltammograms (CVs) revealed that the CNT sheet exhibited a typical carbonaceous anode material while the N-CNT film further displayed a significant incensement of the enclosed area at the voltage of 1 V (Figure 3e; Figure S15 (Supporting Information)), i.e., enhanced intercalation and deintercalation of lithium ions. It is recognized that N-doping not only enhances the electrical conductivity of the material but introduces defects to serve as effective sites for storage of lithium ions, as N is electronegative while Li^+ is electropositive. In addition, the defects are beneficial for the lithium ions to diffuse into the inner space of the electrode material.^[35,36] The charge–discharge curves at current density of 0.1 A g^{-1} also showed a much longer discharge platform from 1 to 0.05 V for the N-CNT film (Figure 3f; Figure S16 (Supporting Information)), which agrees with the CV measurements. The initial reversible capacity of N-CNT film was 516 mAh g^{-1} , about 80% of its first cycle and 5 times of the CNT sheet (Figure S16, Supporting Information).

The rate capacities of N-CNT film and CNT sheet were compared in Figure 3g. When the current densities were increased from 0.2, 0.4, 0.8, and 2 to 4 C, the specific capacities were decreased from 121 to 60 mAh g^{-1} for the CNT sheet and from 516 to 363 mAh g^{-1} for the N-CNT film due to the polarization effect. Obviously, the N-CNT film demonstrated much higher specific capacities at all current densities due to the defective graphene layers that offered more lithiation sites. It also showed higher rate capacity retentions (73% for N-CNT film and 56% for CNT sheet from 0.2 to 4 C) due to the improved electrical conductivity. They displayed the same recovery capability due to the stability of carbon materials. For instance, the N-CNT film had a high specific capacity of 460 mAh g^{-1} when the current was decreased back to 1 C. Noted that the core CNT contributed little in the specific capacity for the N-CNT film because it is difficult for the ions to diffuse through hundreds of N-doped graphene layers to reach the inner CNT. In addition, the bare graphene sheet from the CNT also showed a much lower specific capacity than the N-doped graphene sheet at the sheath.

The cyclic stability of N-CNT film was further tested at a high current density of 4 C (Figure 3h). It showed a high reversible specific capacity of around 370 mAh g^{-1} at the first few cycles, and the specific capacity was further increased gently to 400 mAh g^{-1} in 150 cycles. The lithiation efficiency was relatively low because the micropores, defects and inner layers of N-CNTs cannot be wetted adequately in the first few cycles. Along with the repeated lithiation–delithiation processes, the change of the surface charge distribution promoted the infiltration of electrolyte, so the lithiation efficiency was improved. The capacity started to reduce after 150 cycles due to the irreversible lithiation–delithiation process caused by the channel-block phenomenon.^[37,38] Nevertheless, a specific capacity of 320 mAh g^{-1} had been achieved after 400 cycles. The columbic efficiencies were always almost 100%.

The electrochemical behavior was further studied by examining the N-CNT before and after lithiation by TEM (Figure S17 and S18, Supporting Information). The interlayer space within the N-doped graphene layer was mostly filled after electrochemical lithiation, and the original lattice became fuzzy, particularly

for the layers closer to the edge. This phenomenon suggested that the Li^+ ions entered the walls through the defects from the electrolyte, so the outer layers were more favored. As previously reported, the utilization of the inner layers was limited.^[19–39] With the continuous lithiation–delithiation processes, more inner layers were exploited, but some smaller channels and pores might be blocked and lost the capability of further delithiation. These two opposite effects caused the specific capacity to increase at the first hundred cycles and then decrease in the following cycles (Figure 3h). The other studies on nitrogen-doped CNT materials also suggested that the defects in the walls would create larger specific surface areas and more nanopores, which favored absorption and transport of Li^+ ions.^[20–39] In addition, the N-doped sites were more energetically favorable for Li^+ ions due to a higher electronegativity.^[19–40] The higher electrical conductivity of N-CNT film improved the rate capability especially at a higher current density.

The N-CNT film had been assembled with $\text{LiFePO}_4/\text{CNT}$ films to produce flexible LIBs (Figure 4a). LiFePO_4 was mixed with polyvinylidene fluoride and 1-methyl-2-pyrrolidinone as a slurry in the cathode, and the mixture was painted onto a CNT sheet and dried.^[30–41] The $\text{LiFePO}_4/\text{CNT}$ and N-CNT films were separated by polyethylene, followed by injection of a common electrolyte (LB303). This full LIB showed a specific capacity of 75 mAh g^{-1} at a current of 0.02 mA (Figure 4b). The rate capability was tested with currents of 0.05, 0.1, 0.25, and then back to 0.05 mA (Figure S19, Supporting Information). And the capacity maintained above 70% after 100 cycles charge–discharge process (Figure S20, Supporting Information). In addition, it could stably work under bending and twisting (Figure 4c). A capacity retention of about 60% can be achieved after 100 bending cycles (Figure S21, Supporting Information), and a bended battery shows a comparable cyclic performance with relaxed batteries (Figure S22, Supporting Information).

In summary, a new family of aligned N-CNT films has been synthesized through a chemical vapor deposition. They simultaneously show high mechanical strength, electrical conductivity, and electrochemical activity, for instance, a high specific capacity of 320 mAh g^{-1} with good rate capability has been achieved at a high current density of 4 C after 400 cycles. The N-CNT film can be assembled into a full flexible LIB with stable performances under bending and twisting.

Experimental Section

The aligned CNT sheets were dry-drawn from a spinnable CNT array that had been synthesized by chemical vapor deposition. It was transferred to the tube furnace and then served as a template to further grow the N-CNT film. A gas mixture of argon (110 sccm) and hydrogen (10 sccm) was used as the carrying gas, while acetonitrile was used as the source of both carbon and nitrogen. The growth typically occurred at a temperature of $1060 \text{ }^\circ\text{C}$ with the time from 10 to 90 min. For a half cell, the aligned N-CNT film was used as an electrode to fabricate the LIB without any binder. Here, lithium wafer and commercial LB303 functioned as the opposite electrode and electrolyte, respectively. For a full LIB, an N-CNT film acted as the counter electrode, a CNT sheet served as both current collector and conductive agent, and LiFePO_4 was used as active material. The electrochemical measurements were made at an electrochemical station. The half-cell was charged and discharged within 0–3 V at current densities of 0.1, 0.2, 0.4, 1, 2, and back to

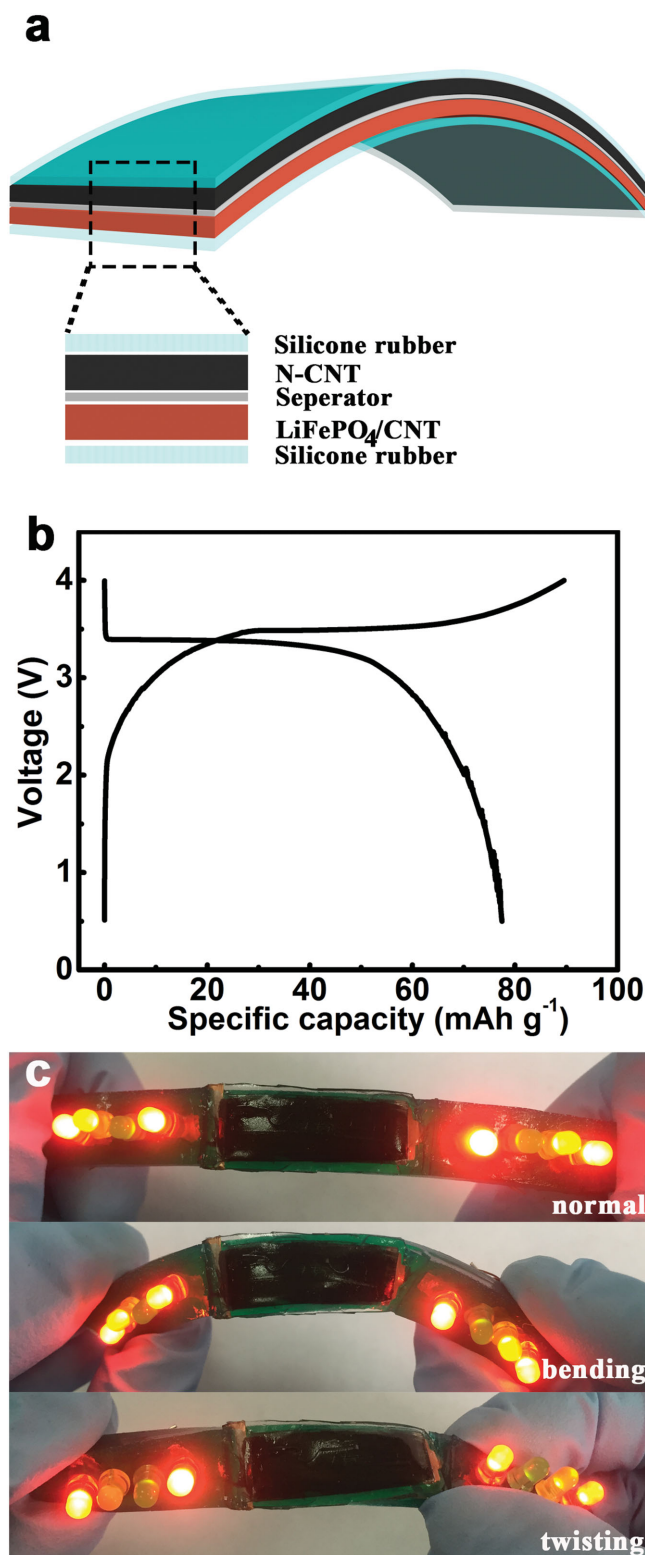


Figure 4. Flexible LIB fabricated from N-CNT and LiFePO₄/CNT films. a) Schematic illustration to the structure. b) Galvanostatic charge and discharge curves at 0.02 mA. c) Photographs of a flexible LIB to power light-emitting diodes before (top) and after bending (middle) and twisting (bottom).

0.5 mA g⁻¹. The cyclic voltammograms were obtained at a scan rate of 0.5 mV s⁻¹.

Supporting Information

Supporting Information is available from the Wiley Online Library or from the author.

Acknowledgments

Z.P. and J.R. contributed equally to this work. This work was supported by NSFC (21225417, 51573027, 51403038), STCSM (15XD1500400, 15JC1490200), and the Program for Outstanding Young Scholars from Organization Department of the CPC Central Committee. This work was supported in part by the Samsung Advanced Institute of Technology (SAIT)'s Global Research Outreach (GRO) Program (IO140919-02248-01).

Received: February 5, 2016

Revised: February 28, 2016

Published online: March 29, 2016

- [1] R. H. Baughman, A. A. Zakhidov, W. A. de Heer, *Science* **2002**, 297, 787.
- [2] Z. Yang, J. Ren, Z. Zhang, X. Chen, G. Guan, L. Qin, Y. Zhang, H. Peng, *Chem. Rev.* **2015**, 115, 5159.
- [3] M. F. L. De Volder, S. H. Tawfick, R. H. Baughman, A. J. Hart, *Science* **2013**, 339, 535.
- [4] B. J. Landi, M. J. Ganter, C. D. Cress, R. A. DiLeo, R. P. Raffaele, *Energy Environ. Sci.* **2009**, 2, 638.
- [5] K. Evanoff, J. Khan, A. A. Balandin, A. Magasinski, W. J. Ready, T. F. Fuller, G. Yushin, *Adv. Mater.* **2012**, 24, 533.
- [6] Y. Hu, X. Li, J. Wang, R. Li, X. Sun, *J. Power Sources* **2013**, 237, 41.
- [7] B. J. Hinds, N. Chopra, T. Rantell, R. Andrews, V. Gavalas, L. G. Bachas, *Science* **2004**, 303, 62.
- [8] H. Lin, W. Weng, J. Ren, L. Qiu, Z. Zhang, P. Chen, X. Chen, J. Deng, Y. Wang, H. Peng, *Adv. Mater.* **2014**, 26, 1217.
- [9] M. Li, Y. Wu, F. Zhao, Y. Wei, J. Wang, K. Jiang, S. Fan, *Carbon* **2014**, 69, 444.
- [10] M. S. Ahmed, D. Kim, S. Jeon, *Electrochim. Acta* **2013**, 92, 168.
- [11] D. Kim, L. Zhu, D. J. Jeong, K. Chun, Y. Y. Bang, S. R. Kim, J. H. Kim, S. K. Oh, *Carbon* **2013**, 63, 530.
- [12] Y. Li, W. Zhou, H. Wang, L. Xie, Y. Liang, F. Wei, J. C. Idrobo, S. J. Pennycook, H. Dai, *Nat. Nanotechnol.* **2012**, 7, 394.
- [13] G. Lota, K. Fic, E. Frackowiak, *Energy Environ. Sci.* **2011**, 4, 1592.
- [14] K. N. Wood, R. O'Hayre, S. Pylypenko, *Energy Environ. Sci.* **2014**, 7, 1212.
- [15] U. N. Maiti, W. J. Lee, J. M. Lee, Y. Oh, J. Y. Kim, J. E. Kim, J. Shim, T. H. Han, S. O. Kim, *Adv. Mater.* **2014**, 26, 40.
- [16] Y. Cao, H. Yu, J. Tan, F. Peng, H. Wang, J. Li, W. Zheng, N. B. Wong, *Carbon* **2013**, 57, 433.
- [17] D. Jana, C. L. Sun, L. C. Chen, K. H. Chen, *Prog. Mater. Sci.* **2013**, 58, 565.
- [18] Q. Shi, F. Peng, S. Liao, H. Wang, H. Yu, Z. Liu, B. Zhang, D. Su, *J. Mater. Chem. A* **2013**, 1, 14853.
- [19] W. H. Shin, H. M. Jeong, B. G. Kim, J. K. Kang, J. W. Choi, *Nano Lett.* **2012**, 12, 2283.
- [20] S. W. Lee, N. Yabuuchi, B. M. Gallant, S. Chen, B. S. Kim, P. T. Hammond, Y. Shao Horn, *Nat. Nanotechnol.* **2010**, 5, 531.

- [21] J. Lim, U. N. Maiti, N. Y. Kim, R. Narayan, W. J. Lee, D. S. Choi, Y. Oh, J. M. Lee, G. Y. Lee, S. H. Kang, H. Kim, Y. H. Kim, S. O. Kim, *Nat. Commun.* **2016**, *7*, 10364.
- [22] D. Ghosh, S. O. Kim, *Electron. Mater. Lett.* **2015**, *11*, 719.
- [23] W. J. Lee, U. N. Maiti, J. M. Lee, J. Lim, T. H. Han, S. O. Kim, *Chem. Commun.* **2014**, *50*, 6818.
- [24] A. M. Gaikwad, B. V. Khau, G. Davies, B. Hertzberg, D. A. Steingart, A. C. Arias, *Adv. Energy Mater.* **2015**, *5*, 1401389.
- [25] Y. Jjiang, A. Kozinda, T. Chang, L. Lin, *Sens. Actuators, A* **2013**, *195*, 224.
- [26] X. Wang, X. Lu, B. Liu, D. Chen, Y. Tong, G. Shen, *Adv. Mater.* **2014**, *26*, 4763.
- [27] J. Ren, Y. Zhang, W. Bai, X. Chen, Z. Zhang, X. Fang, W. Weng, Y. Wang, H. Peng, *Angew. Chem. Int. Ed.* **2014**, *53*, 7864.
- [28] L. Hu, H. Wu, F. La Mantia, Y. Yang, Y. Cui, *ACS Nano* **2010**, *4*, 5843.
- [29] L. Shen, C. Yuan, H. Luo, X. Zhang, K. Xu, F. Zhang, *J. Mater. Chem.* **2011**, *21*, 761.
- [30] W. Weng, H. Lin, X. Chen, J. Ren, Z. Zhang, L. Qiu, G. Guan, H. Peng, *J. Mater. Chem. A* **2014**, *2*, 9306.
- [31] X. Li, J. Yang, Y. Hu, J. Wang, Y. Li, M. Cai, R. Li, X. Sun, *J. Mater. Chem.* **2012**, *22*, 18847.
- [32] G. Ning, C. Xu, Y. Cao, X. Zhu, Z. Jiang, Z. Fan, W. Qian, F. Wei, J. Gao, *J. Mater. Chem. A* **2013**, *1*, 408.
- [33] W. Li, M. Li, M. Wang, L. Zeng, Y. Yu, *Nano Energy* **2015**, *13*, 693.
- [34] Y. Chen, X. Li, K. Park, J. Song, J. Hong, L. Zhou, Y.-W. Mai, H. Huang, J. B. Goodenough, *J. Am. Chem. Soc.* **2013**, *135*, 16280.
- [35] C. Zhang, L. Fu, N. Liu, M. Liu, Y. Wang, Z. Liu, *Adv. Mater.* **2011**, *23*, 1020.
- [36] B. Zhang, Y. Yu, Z. L. Xu, S. Abouali, M. Akbari, Y. B. He, F. Kang, J. K. Kim, *Adv. Energy Mater.* **2014**, *4*, 1301448.
- [37] P. Guo, H. Song, X. Chen, *Electrochem. Commun.* **2009**, *11*, 1320.
- [38] N. Meethong, Y. H. Kao, W. C. Carter, Y. M. Chiang, *Chem. Mater.* **2010**, *22*, 1088.
- [39] V. Meunier, J. Kephart, C. Roland, J. Bernholc, *Phys. Rev. Lett.* **2002**, *88*, 075506.
- [40] T. Sharifi, M. Valvo, E. Gracia-Espino, R. Sandstrom, K. Edstrom, T. Wagberg, *J. Power Sources* **2015**, *279*, 581.
- [41] M. Chen, C. Du, B. Song, K. Xiong, G. Yin, P. Zuo, X. Cheng, *J. Power Sources* **2013**, *223*, 100.